UC Berkeley

Title

Comparisons of heat treatment on the electrochemical performance of different carbons for lithium-oxygen cells

Permalink

https://escholarship.org/uc/item/0j62g8tm

Authors

Guan, Peng
Wang, Guixin
Luo, Chunhui
et al.

Publication Date

DOI

Peer reviewed

AUTHOR QUERY FORM

Dear Author,

Please check your proof carefully and mark all corrections at the appropriate place in the proof (e.g., by using on-screen annotation in the PDF file) or compile them in a separate list. Note: if you opt to annotate the file with software other than Adobe Reader then please also highlight the appropriate place in the PDF file. To ensure fast publication of your paper please return your corrections within 48 hours.

For correction or revision of any artwork, please consult http://www.elsevier.com/artworkinstructions.

Any queries or remarks that have arisen during the processing of your manuscript are listed below and highlighted by flags in the proof. Click on the 'Q' link to go to the location in the proof.
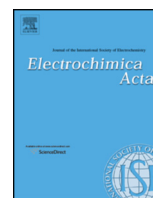
Location in article	Query / Remark: **click on the Q link to go** **Please insert your reply or correction at the corresponding line in the proof**
Q1	Please confirm that given names and surnames have been identified correctly. Please check this box or indicate your approval if you have no corrections to make to the PDF file ☐

Thank you for your assistance.

ARTICLE IN PRESS

Comparisons of heat treatment on the electrochemical performance of different carbons for lithium-oxygen cells

Q1 Peng Guan [a], Guixin Wang [a,*], Chunhui Luo [a], Kangping Yan [a], Elton J. Cairns [b,c], Xueshan Hu [d]

[a] College of Chemical Engineering, Sichuan University, Chengdu 610065, China
[b] Department of Chemical and Biomolecular Engineering, University of California, Berkeley, CA,USA
[c] Environmental Energy Technologies Division, Lawrence Berkeley National Laboratory, Berkeley, CA,USA
[d] Novolyte Technologies Co. Ltd., Suzhou Industrial Park, Suzhou 215123, Jiangsu, China

ARTICLE INFO

ABSTRACT

Lithium-oxygen ($Li-O_2$) cells are a promising power source, and carbons are an attractive non-metal catalyst for air electrodes. To improve the electrochemical performance, various carbons are heated in an inert atmosphere. It is found that heat treatment at 900 °C can differently improve the electrochemical performance of multiwalled carbon nanotubes (CNTs), acetylene carbon black (AB) and activated carbon (AC), but the improvement of CNTs is the most obvious. After heat treatment, the peak current density of the oxygen reduction reaction (ORR) and the 1st discharge capacity of CNTs increase ~30% and ~125%, respectively, while the charge transfer reaction resistance and the Warburg diffusion resistance decrease ~7.0% and ~11.1%, respectively. AC has the highest charge capacities and capacity retention ratio in spite of little influence by heat treatment. The possible mechanism and reasons are analyzed using different techniques. Microstructure is superior to conductivity to enhance the rechargeability and the cyclability, and heat treatment is effective for some carbon materials in improving the electrochemical performance of $Li-O_2$ cells.

© 2014 Published by Elsevier Ltd.

1. Introduction

Lithium-air (Li-air) cells have received considerable attention ranging from fundamental studies to applications as promising power supplies for electric vehicles (EVs) or mobile devices with high specific energy. These cells have significant advantages over conventional electrochemical energy storage and conversion devices for their high theoretical energy density because they use oxygen from the air instead of storing an oxidizer internally, comparable to traditional gasoline engine systems. Because they work using the reduction of oxygen at the cathode, Li-air cells are also called Li-oxygen ($Li-O_2$) cells. According to the Faradic law, a $Li-O_2$ cell can deliver ~5.2×10^3 Wh kg^{-1} (including the weight of oxygen) and 1.1×10^4 Wh kg^{-1} (excluding the weight of oxygen), 5 ~ 10 times more energy than that of state-of-the-art lithium-ion cells [1–9]. However, the development of practical Li-air cells for use in an ambient environment faces many challenges such as the air electrode, the current collector, the electrolyte, the separator and the lithium anode. Air electrodes, where oxygen reduction and evolution reactions take place, are at the heart of the technologies required for rechargeable Li-air cells. Several major obstacles, such as the deposition of discharge products in the pores of air electrodes, passivation by deposits of insulating discharge products, oxygen diffusion transport and reaction kinetic limitations, have to be overcome to achieve higher capacity and longer-life cells [2–12]. Currently, many materials, including Pt and its alloys [2–9,13,14], Au and its alloys [2–9,14], MnO_y [2–9,15–17], FeO_y [2–9,16], CoO_y [2–9,16], $LaMn_{0.6}Fe_{0.4}O_3$ [18], $La_{0.5}Sr_{0.5}CoO_{2.91}$ [19], conducting PEDOT polymers [2–9,20], carbon black [2–9,12], carbon nanotubes and their composites [2–9,21,22], activated carbons [2–11], graphene oxides [2–10], graphenes and their composites [2–9,23,24], have been explored as possible air electrodes.

The microstructure of air electrode notably affects the electrochemical performance of Li–air cells because pores must supply plenty of microchannels for oxygen diffusion to the three-phase reaction interface and rooms for the storage of product deposition during the discharge process. Carbon materials are interesting as emerging and conceptually new advanced catalysts [25]. Therefore, porous carbons are attractive non-metal materials of choice as air electrodes due to their excellent properties such as highly

* Corresponding author. Tel.: +86 28 85406192.
E-mail addresses: guixinwang1@gmail.com, guixin68@yahoo.com (G. Wang).

accessible surface area, unique gas diffusion microchannels, chemical stability, electrical and thermal conductivity, mechanical strength, low weight, plentiful raw materials like waste biomaterials, various allotropes, and environmental compatibility. However, the deposition of reaction products makes it possible to block some pores, hindering gas transport during the discharge process [26]. On the other hand, carbon itself generally exhibits a poor ORR activity in Li-O_2 cells using non-aqueous electrolytes [27]. In order to improve the electrocatalytic activities, different approaches, such as the use of heteroatom doping [24,25,28–31], graphitization [32], and MnO_2 nanoflake coatings [33], have been extensively investigated. Considering the requirements of porous structure and oxygen reduction reaction activity, much research has been conducted on the surface activation treatment of carbons [34,35]. Heat treatment is one of the effective ways to improve the graphitization degree, and modify the microstructure and surface chemistry of carbons [36–38], but its influence on the electrocatalytic activities of different carbons in a Li-O_2 cell is still not clear.

In this study, comparisons of heat treatment on the electrocatalytic performance of various carbon materials have been carried out using different methods, and the possible mechanisms and reasons have been analyzed using combined techniques.

2. Experimental Section

2.1. Heat treatment of different carbons

High surface area is one of the important properties of a material with a well-developed pore structure that benefits gas diffusion and supply of reaction sites. According to the references [34,38], heat treatment at 900 °C significantly increases the surface area of carbon, so 900 °C was chosen as the heat treatment temperature for this work. Three kinds of carbon materials, i.e. multiwalled CNTs produced from methane, commercial AC from coconut shells and AB from acetylene [39], were heat treated in a quartz tube furnace where nitrogen gas was passed through at a flow rate of 100 sccm. With a temperature increase rate of 10 °C min^{-1}, the samples were heated to 900 °C and kept at this temperature for 1.5 h, and then naturally cooled to room temperature in the furnace. These samples were ground in an agate mortar for characterization. The as-obtained heat treated CNTs, AC and AB at high temperature were denoted as HT-CNTs, HT-AC and HT-AB, respectively.

2.2. Materials characterization

The crystalline structure of the carbons was verified by X-ray diffraction (XRD, Philips X'Pert pro MPD) using Cu-Kα radiation in the range from 10 to 70° at a scan rate of 0.04° s^{-1}. The surface functional groups on the carbons were evaluated by Fourier transform infrared spectroscopy (FTIR) on a thermo Nicolet Magna IR 560 spectrometer in the range of 900 ~ 3800 cm^{-1} using the KBr pellet method, and all spectra were obtained using 0.05 cm^{-1} resolution. Nitrogen adsorption-desorption isotherms were determined at 77 K on an Autosorb SI surface area & pore size analyzer (Quantachrome instruments, USA). Samples were pretreated at 300 °C for 3 h to degas them under vacuum prior to adsorption measurements. The specific surface areas of the samples were calculated with the Brunauer-Emmett-Teller (BET) equation in a relative pressure range from 0.06 to 0.35, whereas the pore size distribution (PSD) was obtained by the adsorption branch of the isotherms using the Barrett-Joyner-Halenda (BJH) model. The total pore volume (V_t) was estimated from the adsorbed amount at a relative pressure (P/P$_0$) of 0.99. X-ray photoelectron spectroscopy (XPS) was performed on a Kratos XSAM800 photoelectron spectrometer with Al-Mg X-ray radiation at 12 kV × 15 mA under vacuum. All the binding energies were corrected based on the internal standard of the C1s peak position at 284.8 eV.

2.3. Electrochemical evaluation

To increase the cell operating voltage and thus the energy density, the electrocatalytic performance of the carbons were evaluated in an organic electrolyte with a wide electrochemical potential window using self-made two-electrode Li-air cells with gas channels. The working electrode was prepared by coating a carbon slurry onto a clean nickel foam using a doctor blade, and being dried at 100 °C in a vacuum oven before being cut into wafers of 1.9 cm diameter. The carbon slurry with a composition of 90 wt.% carbon and 10 wt.% polytetrafluoroethylene (PTFE) was prepared by stirring and grinding the mixture of carbon powder and PTFE emulsion (solid content = 60 wt.%, Shanghai 3F New Material Co.) diluted with an appropriate amount of deionized water. In order to test its own performance of each carbon, no conductive carbon was added to make the slurry. Porous nickel foam was used as not only the support for the active materials, but also the storage for the discharge products, current collector, and gas channels for oxygen transfer. These wafers with a loading density of ~0.57 mg (carbon materials)/cm^{-2} (apparent surface area of nickel disc) were further dried at 100 °C for 12 hours in a vacuum drying oven for use as working electrodes. Pure lithium foil was used as the counter and reference electrodes. 1.0 M LiPF$_6$ dissolved in tetraethylene glycol dimethyl ether (Novolyte Technologies Co. Ltd., China) solution was used as the non-aqueous electrolyte, and its amount in each electrode was controlled around 0.08 ml using a precision graduated syringe. The cells were assembled by sandwiching a Celgard 2300 microporous separator between the working electrode and the metal lithium in an argon-filled glove box. The side of the cell with open vent holes is adjacent to the carbon cathode to allow for oxygen transfer, and the other side is adjacent to the lithium foil with air tightness to prevent lithium corrosion. The electrochemical performance of the cells was evaluated in a dry oxygen atmosphere at room temperature using different techniques, including galvanostatic discharge/charge method, cyclic voltammetry (CV), and electrochemical impedance spectroscopy (EIS). The discharge/charge tests were conducted on a battery testing instrument (Neware Technologies Co. Ltd., China) with a constant current density of 70 mA (g carbon)$^{-1}$ in a potential window of 2.0 ~ 4.2 V vs. Li$^+$/Li. CV measurements of the Li-O_2 cells were carried out at a scan rate of 0.2 mV s^{-1} between 2.0 and 4.2 V vs. Li$^+$/Li on a PAR 273A potentiostat/galvanostat (Princeton Applied Research, USA). EIS measurements of the fresh Li-O_2 cells were performed over a frequency range of 10 mHz ~ 100 kHz with a sinusoidal excitation voltage amplitude of 10 mV on an electrochemical workstation consisting of the PAR273A and a signal recovery model 5210 lock-in-amplifier controlled by Powersuite software. The impedance curves were fitted using Zsimpwin and Zview software [40,41].

3. Results and discussion

In order to understand the influence of heat treatment on the electrochemical performance of carbon materials and to improve the energy density of Li-O_2 cells beyond that available with aqueous electrolytes, these carbons were evaluated using an organic electrolyte with a wide electrochemical window. Fig. 1 shows the galvanostatic discharge/charge curves of the Li-O_2 cells prepared with different carbon materials, and the key values are summarized in Table 1. From the testing results, heat treatment differently improves the discharge/charge capacities and capacity retention of all carbons in the organic electrolyte. The sequence of the initial

Table 1
Comparisons of heat treatment on the capacities of different carbon materials.

Materials	1st discharge (mAh/g)	1st charge (mAh/g)	2nd discharge (mAh/g)	2nd charge (mAh/g)
CNTs	1001	140	174	69
HT-CNTs	2255	341	245	128
AB	1839	74	73	36
HT-AB	1974	77	74	37
AC	1592	677	323	258
HT-AC	1770	781	365	306

ORR activity of the pristine carbons is AB > AC > CNTs, but it changes to CNTs > AB > AC after heat treatment. HT-CNTs have the highest initial discharge capacity, but the charge capacity and the 2nd discharge capacity are low, which may be from the dead-lithium during the 1st discharge process. No matter how much heat treating is done, the sequence of the charge capacity and the capacity retention of the carbons is AC > CNTs > AB. Under the same conditions, heat treatment increases the initial discharge capacity of CNTs from 1000 to 2254 mAh g^{-1}, and the initial charge capacity of CNTs from 140 to 341 mAh g^{-1}, as shown in Fig. 1a. At the same time, the initial discharge capacities of AB and AC have been increased ~7.3% to reach 1974 mAh g^{-1} and ~11.2% to reach 1770 mAh g^{-1}, respectively, as shown in Fig. 1b and c. The discharge capacity retention ratios of the 2nd cycle to the 1st cycle of the heated CNTs, AB and AC are ~10.9%, ~3.7% and ~20.1%, respectively. The fade reasons are very complex, and one of them may originate from the blocked microstructure by the product of lithium oxides which have not completely decomposed during the charge process because of the low coulombic efficiency. On the other hand, these carbons have definite rechargeable properties despite the large fade between the first two cycles. Heat treatment differently decreases all the charge potential plateaus of various carbons, and increases the discharge potential plateaus of CNTs, but has little influence on that of AB and AC, indicating heating treatment differently decreases the medium potential difference between discharge curves and charge curves. The heated samples all have the stable discharge potential plateaus at ~2.6 V during the 1st discharge process, similar to that of the lithium-O$_2$ cells using carbon black [12], CNTs [21], SWNT/CNF buckypapers [22] or graphene [22,23], corresponding to the reaction of O$_2$ with Li$^+$ ions to form lithium oxides. Noticeably, the potential plateaus are much stable and higher than that of CNTs for lithium-ion batteries besides the higher discharge capacity [42], indicating the energy storage mechanism of lithium-oxygen cells is different from the lithium insertion/extraction mechanism of lithium-ion batteries. The capacity retention and the charge behavior of AC are better than that of CNTs or AB in spite of the low initial discharge capacity and little influence by heat treatment, which may be from the developed microstructure with a high specific surface area of 2000 m^2 g^{-1} [39].

To investigate the influence of heat treatment on the interface behavior of the carbons, the EIS curves of the fresh cells are compared under the same conditions with an open circuit potential of ~3.1 V. The Nyquist plots of various carbons, along with the equivalent circuit model used for EIS data fitting are presented in Fig. 2. All curves consist of a depressed semicircle in high-to-medium frequency region and an oblique line in low frequency region, indicating a similar electrode reaction process. The intercept of the curve on the Z' real axis in high frequency region reflects the Ohmic resistance. The depressed semicircle in the high-to-medium frequency corresponds to the interface film and charge transfer reaction impedances, which is related to the electrode reaction kinetics. The oblique line in the low frequency region is associated with the Warburg impedance, which is relevant to the semi-infinite diffusion and mass transport process of lithium ions. Except that of AB, the knee frequency at the mixed-control region of the charge transfer reaction and mass transport of CNTs or AC increases after heat treatment, indicating that the electrode reaction kinetics have been improved. The EIS experimental data, subjected to a nonlinear least-square fitting procedure, can be fitted well by the equivalent circuit model of R$_s$(Q$_i$R$_i$)(Q$_d$(R$_{ct}$W)) supplied in Fig. 2d, and the theoretical impedance plots match exactly with the experimental curves. Considering the nonhomogeneity such as porosity, roughness and geometry in the electrode system, constant phase element (CPE) Q is used to substitute for capacitance C [17,40,41]. A depressed semicircle will be formed when the CPE is placed in parallel with a resistor, as shown in Fig. 2a-c. In the equivalent circuit, R$_s$ is the solution Ohmic resistance which follows the Ohm's law, including the contributions from electrolyte, temperature and the geometry of the area in which current is carried; R$_i$ is the interfacial resistance between active material particles and other adjacent substances (such as particles, electrolyte, current collector, and binder), and Q$_i$ is the constant phase element of the interface film; R$_{ct}$, Q$_d$, and W are the charge transfer reaction resistance of electrode, the constant phase element of the three-phase interface of O$_2$, electrolyte and active material, and the general Warburg diffusion impedance which concerns the semi-infinite chemical diffusion of lithium ions and gas in the air electrode, respectively. R$_{ct}$ and W share one constant phase element Q, indicating that charge transfer reaction and diffusion take place at the three-phase interface. The fitted results of the EIS curves are summarized in Table 2. The high R$_i$, R$_{ct}$ and W values of CNTs and HT-CNTs may be from the complex microstructure, the electron jump between different layers and the long diffusion path because CNTs are made of many cylinder layers with a long length [17,21,39,41]. The low diffusion resistance of AC is from its developed microstructure with plenty of microchannels for gas transport. Heat treatment can decrease the charge transfer reaction impedance of these carbons to different degrees, and the values of R$_{ct}$ of CNTs, AB and AC decrease ~7.0%, ~7.8% and ~2.3%, respectively, which further confirms the improvement of reaction kinetics of different carbons by heat treatment.

From above results, it can be seen that heat treatment has a significant influence on the electrochemical performance of CNTs. To further investigate the ORR activity of the carbon in the organic electrolyte, cyclic voltammetry measurements of the Li-O$_2$ cells were conducted, as shown in Fig. 3. The CV curves of the CNTs have no quasi-rectangular capacitive properties, and the shape is similar to that of carbon black in the lithium-oxygen cells using organic electrolyte [43], different from that in aqueous electrolyte (See Figure S1, Supporting Information), that of the lithium-ion batteries [42] or that of the supercapacitors using the similar carbon

Table 2
Influence of heat treatment on the impedances of different carbon materials.

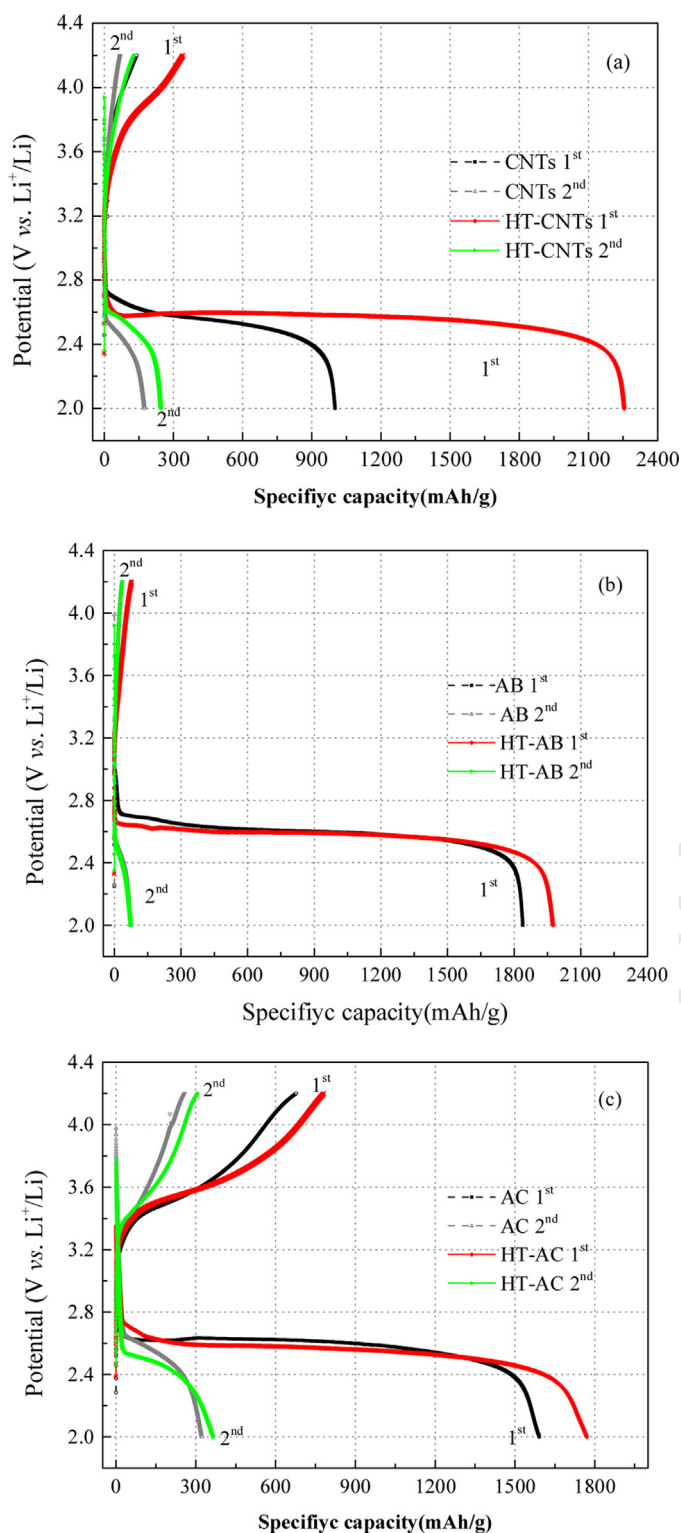| Materials	R$_s$ (ohm)	R$_i$ (ohm)	R$_{ct}$ (ohm)	W (ohm)
CNTs	25.7	120.8	178.2	329.5
HT-CNTs	12.5	111.6	165.7	292.9
AB	40.8	17.2	170.3	315.7
HT-AB	16.6	16.9	157.1	293.2
AC	14.7	28.2	196.1	148.8
HT-AC	35.5	52.6	191.5	147.6

Fig. 1. Influence of heat treatment on the galvanostatic discharge/charge curves of different carbons in the organic electrolyte.

Fig. 2. (a) Nyquist plots of the Li-O$_2$ cells using (a) CNTs and HT-CNTs, (b) AB and HT-AB, (c) AC and HT-AC, and (d) corresponding equivalent circuit model.

materials [39]. According to the references [44,45], O$_2$ reduction proceeds in a stepwise fashion to form O$_2^-$, O$_2^{2-}$, and O^{2-} intermediates in Li$^+$-containing electrolytes, and the product is a mixture of Li$_2$O$_2$ and Li$_2$O. The insulative lithium oxides cover the surface of carbon electrode to decrease the Helmholtzs layer between electrolyte and active materials, so the energy storage based on electric double-layer mechanism is not obvious, which results in no visible
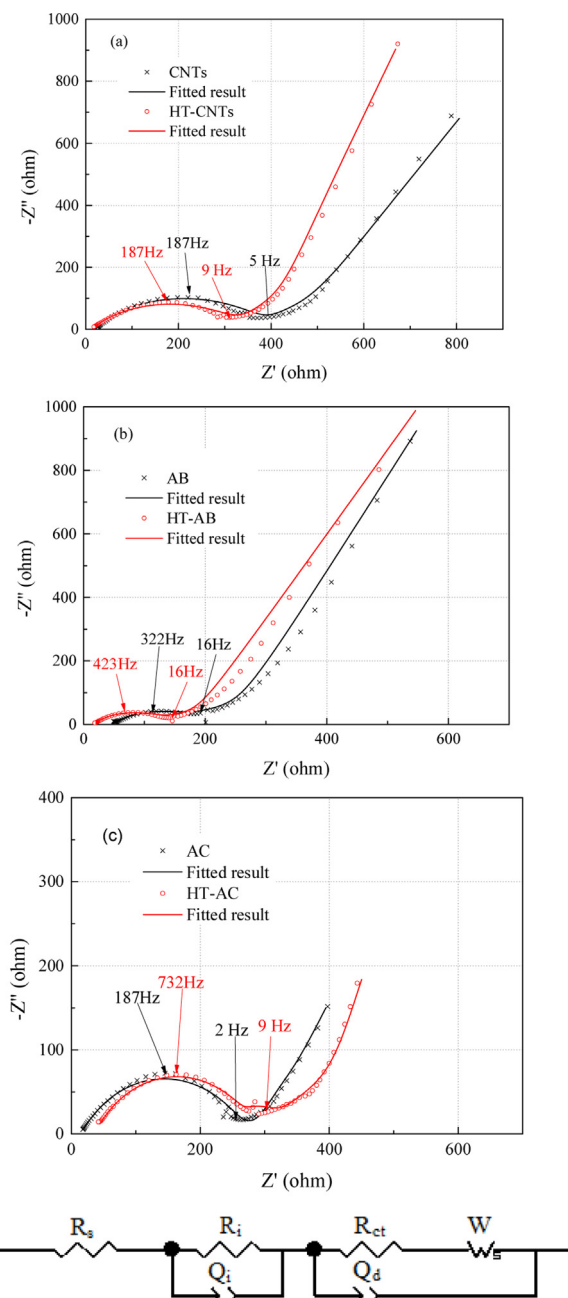
capacitance behavior in the CV curves using organic electrolyte. This also indicates the energy storage of carbon air electrodes in lithium-oxygen cells using organic electrolyte is mainly based on redox reactions, i.e. ORR and oxygen evolution reaction (OER) [2–9]. The reduction peak of the pristine CNTs is not sharp, but the peak becomes very obvious after heat treatment. The reduction peak position of the HT-CNTs is at ~2.2 V, and the reduction current density increases ~30%, indicating that the ORR activity of CNTs has been improved by heat treatment, which is consistent with above results. Carbons have interesting catalytic performance [2–12,20–23,30], and the potentials of the catalytic peaks can be given in 3 ways [46]: 1) the onset, 2) the half-wave, and 3) the pinnacle of the peaks. After heat treatment, the half-wave potential and the pinnacle potential move positively if we consider the smooth transition of the ORR peak of the pristine carbon, but the onset
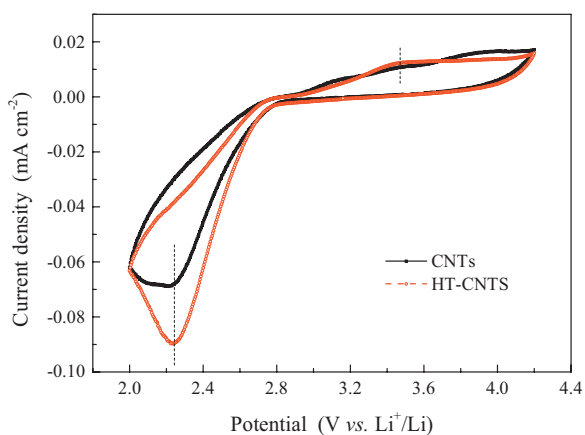
Fig. 3. Comparisons of the CV curves of the Li-O$_2$ cells using CNTs and HT-CNTs in the organic electrolyte.

potential of the carbon has no visible positive movement, similar to that of the N-doped graphene catalysts [24]. The different ORR activities are attributed to the carbon catalysts because the other conditions are same. Therefore, heat treatment can improve the ORR activities of carbon materials, especially for CNTs, which will be analyzed with regard to the possible aspects affected by heat treatment, such as conductivity, surface chemistry, N elemental doping and microstructure.

The influence of heat treatment on the XRD patterns of different carbon materials is shown in Fig. 4. The curves of the heat treated carbons almost coincide with that of the pristine one, indicating that heat treatment at 900 °C has few effects on the crystalline structure and interlayer spacing of various carbons. Compared to AB, AC and their heated samples, CNTs and HT-CNTs have an excessive (004) peak at ~53°, and the (002) peak is sharp and outstanding besides the slight shift of the (002) and (100) peak positions, indicating that the crystalline structure of these carbons is different. CNTs and HT-CNTs have characteristics including an obvious sharp peak at ~26°, weak peaks at ~43° and at ~53°, respectively corresponding to the (002), (100) and (004) faces of the hexagonal graphitic carbon, which indicates a high graphitization degree that corresponds to a good electronic conductivity [47]. However, the (002) peak of AB and HT-AB becomes broad and the (002) peak of AC and HT-AC becomes almost no visible besides the absence of the (004) peak, implying the breaking of the inter-planar bonds of carbon, which indicates AC and HT-AC are inferior to AB and HT-AB to have a low graphitization degree which results in poor conductivity [39,47]. The (002) peak intensity of AB shows a small increase after heat treatment, indicating that heat treatment slightly improves the conductivity. The significant decrease in the intensity of the (002) peak compared to that of CNTs or AB shows that an amorphous structure is dominant for AC, and the (002) peak will increase until the heating temperature is over 1800 °C [38,48]. On the other hand, no visible shift of (002) peak indicates that there is no N doping to the carbon during the heat treatment process in N$_2$ atmosphere, which is further demonstrated by XPS latter. Therefore, the electric conductivity sequence of the carbons and their heat treated samples is CNTs > AB > AC, and the improvement of the graphitization degree of carbons is not obvious after heat treatment at 900 °C.

Surface functional group will affect the electrochemical performance of carbons by changing the dispersion, conductivity and wettability of electrolyte [49]. In order to identify the changes of the surface functional group of carbons after heat treatment, the typical FTIR spectra are shown in Fig. 5. All carbons show strong and broad peaks at around 3430 cm^{-1} and 1120 cm^{-1}, which correspond to the stretching mode of O-H and C-O, respectively. The weak peaks
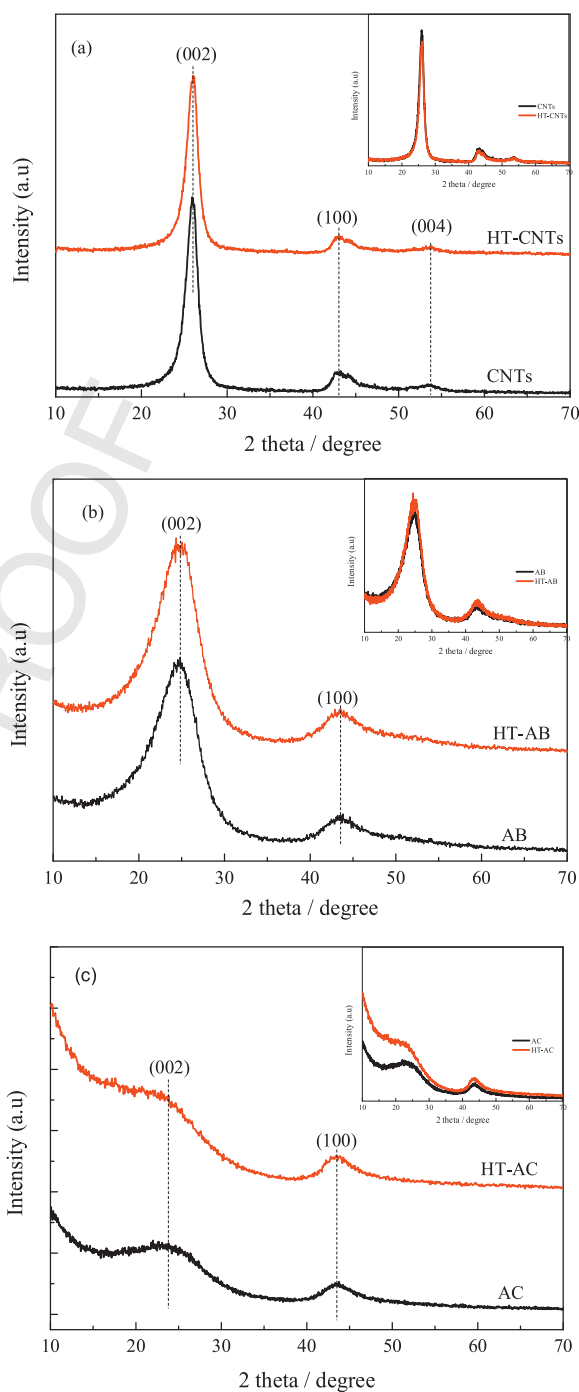

Fig. 4. XRD patterns of different carbon materials (a) CNTs and HT-CNTs, (b) AB and HT-AB, and (c) AC and HT-AC.

at around 2920 cm^{-1} and 1410 cm^{-1} are attributed to the stretching vibrations of asymmetric CH$_2$ and C-OH, respectively. The peaks ranging from 1580 cm^{-1} to 1640 cm^{-1} are the characteristic C = C stretching [50]. From the FTIR peak intensities and positions, the type and amount of the surface functional groups of CNTs and AC are similar, which are much more than that of AB. Compared to the pristine samples, the heat treated samples have no obvious peak changes, indicating the type and amount of surface functional group remain stable. Therefore, the dispersion, the conductivity and the wettability of carbons are similar after heat treatment at 900 °C.

N-doping can improve the catalytic activity of carbon [23,24,27–30], so XPS was conducted to determine whether N
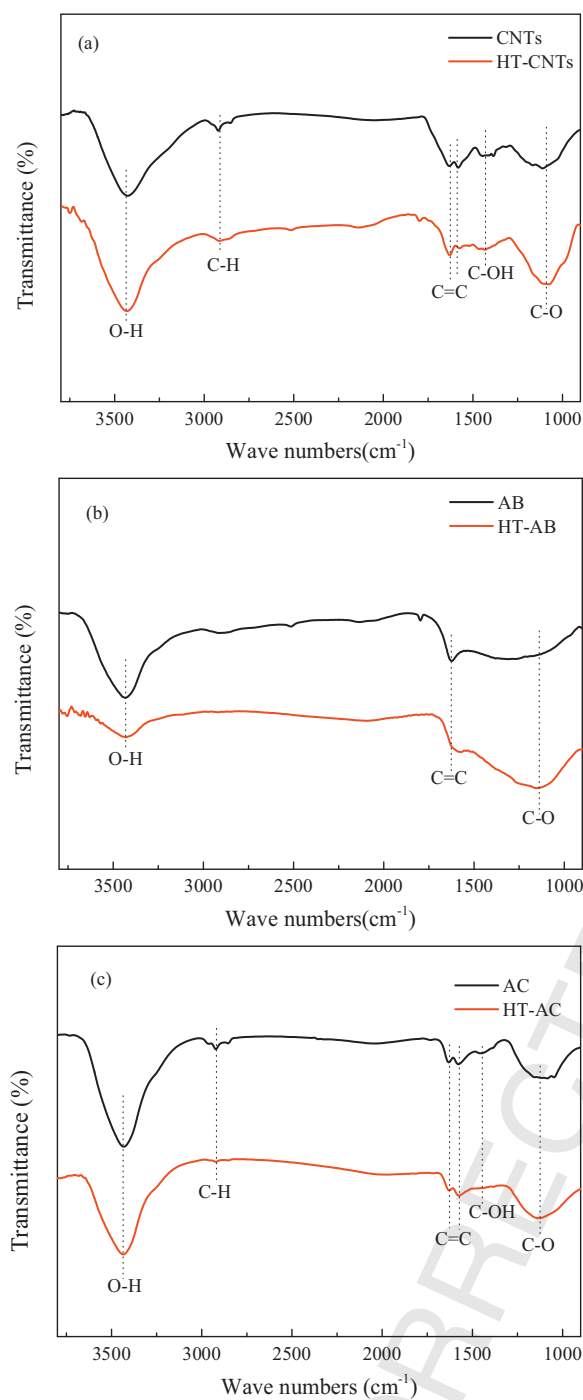
Fig. 5. FTIR spectra of different carbon materials (a) CNTs and HT-CNTs, (b) AB and HT-AB, and (c) AC and HT-AC.

Fig. 6. XPS spectrum of the heated CNTs.

dopes the carbons for enhancing the electrochemical performance since the heat treatment was carried out in a N_2 atmosphere. Because the improvement of the electrochemical performance of CNTs is the most obvious, the composition and elemental chemical state of the heated CNTs were examined by XPS, and the full-scale spectrum is shown in Fig. 6. Noticeably, no nitrogen peak can be detected in the XPS curve, indicating that there is no N doping to the carbon during the heat treatment in N_2 atmosphere at 900 °C, which is due to the chemically extremely unreactive nitrogen molecule. The O is from the surface group of the pristine CNTs which were purified by refluxing with a hot HCl solution, agreeing with above FTIR results. From the semi-quantitative analysis result of XPS,
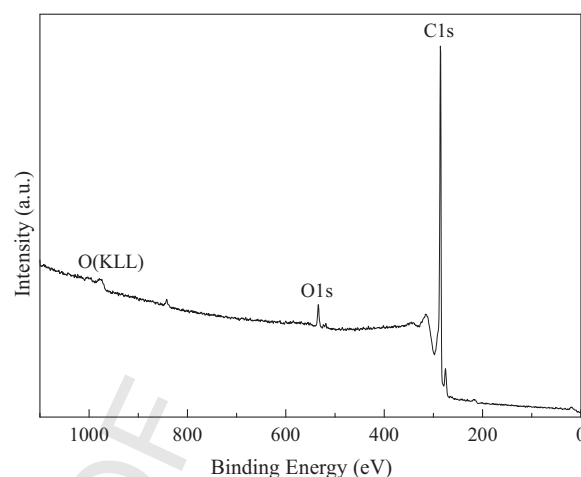
the atomic contents of C and O are 97.4% and 2.6%, respectively. Therefore, there is no contribution of N doping to the improved performance.

According to the above analysis results, the great improvement of the ORR activities is mainly from the improved microstructure because the conductivity and surface functional groups change little as well as there is no N-doping contribution. As for the CNTs with the greatest improvement of performance, the microstructure was evaluated by the BET method at 77 K. The adsorption/desorption isotherms and pore size distribution of CNTs and HT-CNTs are compared in Fig. 7, and the physical and structural parameters are summarized in Table 3. From Fig. 7(a), both samples exhibit typical type-IV N_2 sorption isotherms with distinct H3 hysteresis loops that relate to slit-shaped pores, indicative of a mesoporous characteristic [19,51]. From Fig. 7(b), the pore size distributions of both CNTs and HT-CNTs focus on around 3.8 nm which is in the mesoporous range. The curves show that heat treatment changes the sorption isotherms from $P/P^0 = 0.45$ as well as the BJH pore size distributions. HT-CNTs exhibit a slight adsorption hysteresis phenomenon that is due to the capillary condensation of nitrogen in the mesopores of carbon, indicative of the increase of mesopores. A vertical rise in the location of isothermal curve suggests a volume increase of nitrogen gas adsorption for the pristine CNTs, indicating a decrease in pore volume of the heat-treated carbon. The microporous volume ratio and mesoporous volume ratio were calculated using the α_s-method from desorption and integration from the pore size distribution curve [51], respectively, and the calculated ratios are summarized in Table 3. The value of dV/dD in the pore size range from 3 to 16 nm of heat treated carbon is significantly higher than that of pristine CNTs, indicating that heat treatment improves the mesoporous ratio, which is confirmed by the increased ratio of mesopore volume to total pore volume from 61.11% to 66.81% after heat treatment. Therefore, heat treatment at 900 °C improves the pore microstructure of CNTs, and the ratio of mesopore volume to total pore volume and the BET surface area increase ~5.7% and ~24.7%, respectively, while the total pore volume, the ratio of micropore volume to total pore volume, the ratio of macropore volume to total pore volume, and average pore width decrease ~13%, ~0.1%, ~5.6% and ~31%, respectively. The improvement of the pore microstructure of CNTs by heat treatment is from the collapse of some macropores and the breakdown of some micropores because of the increase of mesoporous ratio and surface area as well as the decrease of pore volume, pore size, microporous ratio and macroporous ratio. At the same time, heat treatment may open some dead pores and increase the defects to enhance the adsorption surface area and the reaction active sites. The balance of micropores,

Table 3
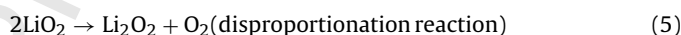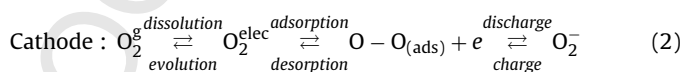Influence of heat treatment on the textural properties of different carbon materials.

Materials	S_{BET} (m^2 g^{-1})[a]	V_{total} (cm^3 g^{-1})[b]	V_{mic}/V_{total} (%)[c]	V_{mes}/V_{total} (%)[d]	V_{mac}/V_{total} (%)	Average pore diameter (nm)[e]
CNTs	149.50	0.54	0.16	61.11	38.73	14.55
HT-CNTs	186.40	0.47	0.05	66.81	33.14	10.12

[a] Apparent surface areas were calculated by multipoint BET method at the relative pressure range of 0.06~0.35.
[b] Total pore volume from adsorption isotherms at P/P$_o$ = 0.99.
[c] α_s-method from desorption
[d] integration method from the pore size distribution curve
[e] BJH method from desorption

mesopores and macropores play an important role in enhancing the electrochemical performance, and more mesopores can effectively improve the discharge capacity of lithium oxygen cells because more mesopores can act as more available gas channels and provide more spaces for the storage of discharge products to allow free oxygen transfer. Furthermore, highly accessible surface area will effectively supply plenty of adsorption and reaction sites for oxygen molecules, which are significant for the improvement of the electrochemical performance of air electrodes and their Li-O$_2$ cells [12]. Therefore, the pore microstructure of carbon plays a critical role in the storage and distribution of lithium oxide product, intensification of mass and heat transport, enhancement of gas diffusion and active sites for electrode reaction.

As for the air electrode reaction of Li-O$_2$ cells, O$_2$ must firstly diffuse into the electrolyte and adsorb to the surface of wetted porous carbons, and then get electrons from the lithium anode under the electromotive force of the potential difference between Li metal and carbon to form oxygen anion intermediates that will further react with lithium ions to produce lithium oxides of Li$_2$O$_2$ and Li$_2$O

during the discharge process [44,45,52]. When the cell is charged, the product will decompose to form Li and O$_2$ for cycling. Hard-soft acid-base theory has been used to elucidate the observed behavior of oxygen reaction [45], and the possible electrode reaction mechanism has been provided as follows [44,45,52].

$$\text{Anode}: \text{Li} - e \underset{charge}{\overset{discharge}{\rightleftarrows}} \text{Li}^+ \tag{1}$$

$$\text{Cathode}: O_2^g \underset{evolution}{\overset{dissolution}{\rightleftarrows}} O_2^{elec} \underset{desorption}{\overset{adsorption}{\rightleftarrows}} O-O_{(ads)} + e \underset{charge}{\overset{discharge}{\rightleftarrows}} O_2^- \tag{2}$$

$$O_2^- + \text{Li}^+ \rightarrow \text{LiO}_2 \tag{3}$$

$$\text{LiO}_2 + \text{Li}^+ + e \rightarrow \text{Li}_2O_2 \tag{4}$$

$$2\text{LiO}_2 \rightarrow \text{Li}_2O_2 + O_2 (\text{disproportionation reaction}) \tag{5}$$

$$\text{Li}_2O_2 + 2\text{Li}^+ + 2e \rightarrow 2\text{Li}_2O \tag{6}$$

Therefore, the whole cathodic reaction can be expressed as

$$2x\text{Li}^+ + O_2 + 2xe \underset{charge}{\overset{discharge}{\rightleftarrows}} 2\text{Li}_x O(1 < x < 2) \tag{7}$$
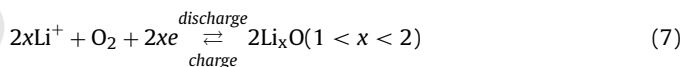
When x = 1, the product is Li$_2$O$_2$, so the reaction is $O_2 + 2\text{Li}^+ + 2e \underset{charge}{\overset{discharge}{\rightleftarrows}} \text{Li}_2O_2$;

When x = 2, the product is Li$_2$O, so the reaction is $O_2 + 4\text{Li}^+ + 4e \underset{charge}{\overset{discharge}{\rightleftarrows}} 2\text{Li}_2O$.

Thus, proper pore size distribution is necessary for oxygen diffusion, and a high accessible surface area is needed to supply more adsorption and reaction sites. At the same time, the produced lithium oxides will deposit on the surface of the carbon or accumulate in the pores to limit the oxygen diffusion and accessibility to the electrode surface for further reaction, which will result in the incomplete utilization of the carbon cathode to decrease the electrochemical performance (even terminate the electrode reaction under serious conditions). Therefore, large size pores are required for lithiation product storage and oxygen diffusion. However, there is a conflict between large size pores and high surface area. So, available pores with proper size distribution and high accessible surface area should compromise to reach a balance for enhancing the electrochemical performance of the porous air electrode, which can be realized by the optimization of pore microstructure using heat treatment.

Consequently, the enhanced electrochemical performance of CNTs is mainly a result of the improvement of mesopore volume and accessible surface area by heat treatment at 900 °C. Heat treatment can produce positive effects like opening the closed dead-end pores produced during the carbon production process, creation of new voids on the surface and pore walls, growth of surface defects and intrinsic lacunae in size and quantity on the tube walls and thinning of the walls [33]. The increase of mesopores and surface area provides additional oxygen diffusion channels for improving oxygen transport as well as spaces for the electrode reaction and
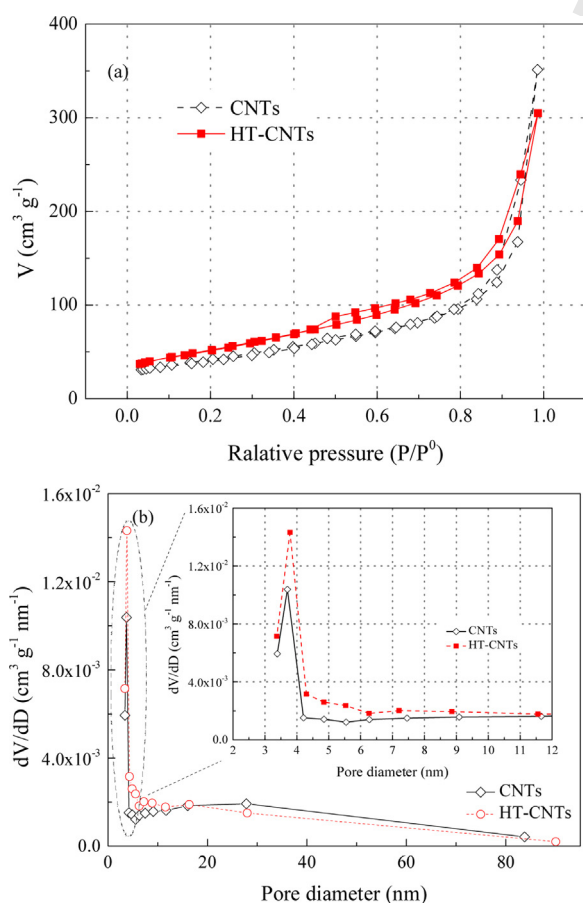

Fig. 7. (a) N$_2$ adsorption-desorption isotherms curves, and (b) pore size distributions of CNTs and HT-CNTs.

storing the solid discharge products on the cathode to enhance the ORR activities, in good agreement with other results [12,53]. Furthermore, heat treatment will also benefit the atomic arrangement to enhance electron flow, break a portion of the C-C bonds to cause carbon atoms dissociation and tube compartments breakage (even result in the creation of interlinks and the surface reconstruction [54]). On the other hand, the lithium product of Li_2O_2 is insulating [44], which will increase the charge transfer resistance to produce a high electrochemical reaction polarization. CNTs with good conductivity can decrease the disadvantages of the insulating intermediate products. In addition, CNTs are superior to perfect hexagonal carbon rings in absorbing O_2 and lithium ions at the edge and other imperfections in the sidewalls [55,56], which leads to numerous activated reaction sites for ORR at the edges or defects of the carbon surface. Therefore, heat treatment will enhance the ORR activities of carbons, and the improvement of CNTs is the most obvious. Further work on optimizing carbon post treatment (such as heat treatment temperature, time and atmosphere, proper pore size distribution, accessible surface area, surface chemistry, conductivity and heteroatom doping) and carbon composites to improve the cycle performance of the Li-oxygen cells is under investigation.

4. Conclusion

In summary, different carbons, including CNTs, AB, and AC, have exhibited specific rechargeable performance as the cathodes of Li-O_2 cells, and heat treatment at 900 °C can differently improve their electrochemical performance. As for the heated samples using the organic electrolyte, the 1st discharge capacities of CNTs, AB and AC increase ~125%, ~7.3%, and ~11.2%, respectively, while the charge transfer reaction resistances of CNTs, AB and AC decrease ~7.0%, ~7.8% and ~2.3%, respectively. HT-CNTs have the highest initial discharge capacity, while AC without/with heat treatment has the highest charge capacity and the best cyclability in spite of the slight enhancement by heat treatment. The discharge/charge properties, EIS, crystalline structure and surface chemistry of the heated carbons were compared, and the possible reasons for the improvement by heat treatment have been analyzed from different aspects. After heat treatment, XRD results show that the crystal structure of the carbons changes little, FTIR spectra indicate that the surface functional groups on the carbons have no visible changes, and XPS result confirms that there is no N doping. As for the CNTs with the most obvious improvement, the ratio of mesopore volume to total pore volume and the BET surface area increase ~5.7% and ~24.7%, respectively, while the total pore volume, the ratio of macropore volume to total pore volume, and average pore width decrease ~13%, ~5.6% and ~31%, respectively. The experimental results show that ORR activities are mainly affected by the pore microstructure and conductivity of the carbons, and microstructure is much more important than conductivity to enhance the rechargeability and cyclability of carbons in spite that conductivity enhances the ORR activities. The capacity retention is determined by the microstructure which favors the adsorption and the reaction of O_2 and allows the compatibility between gas diffusion and storage of discharge products, and initial discharge capacity is affected by the graphitization degree that is closely related to conductivity.

The experiments demonstrate that the selection of carbons with proper heat treatment appears to be a key factor for enhancing the ORR activities, and pore microstructure as well as graphitization degree is of extreme significance for them. In spite of the specific rechargeable properties of carbons, the electrocatalytic performance of carbons need to be further improved by optimizing the microstructure, graphitization degree, surface chemistry, heteroatom doping, surface coating and forming composites.

Consequently, carbons will become competitive as a green catalyst, and heat treatment is a feasible and effective way to enhance the ORR activities by improving the microstructure, which is beneficial to the exploration and applications of promising non-metal catalysts in enhanced energy conversion of Li-O_2 cells.

Appendix A. Supplementary data

Supplementary data associated with this article can be found, in the online version, at http://dx.doi.org/10.1016/j.electacta.2014.02.079.

References

[1] K. Abraham, Z. Jiang, Journal of The Electrochemical Society 143 (1996) 1–5.
[2] G. Girishkumar, B. McCloskey, A. Luntz, S. Swanson, W. Wilcke, The Journal of Physical Chemistry Letters 1 (2010) 2193–2203.
[3] A. Kraytsberg, Y. Ein-Eli, Journal of Power Sources 196 (2011) 886–893.
[4] P.G. Bruce, S.A. Freunberger, L.J. Hardwick, J.M. Tarascon, Nat Mater 11 (2012) 19–29.
[5] F. Cheng, J. Chen, Chemical Society Reviews 41 (2012) 2172–2192.
[6] Y. Shao, S. Park, J. Xiao, J.-G. Zhang, Y. Wang, J. Liu, Acs Catalysis 2 (2012) 844–857.
[7] M.A. Rahman, X. Wang, C. Wen, Journal of The Electrochemical Society 160 (2013) A1759–A1771.
[8] Y.-C. Lu, B.M. Gallant, D.G. Kwabi, J.R. Harding, R.R. Mitchell, M.S. Whittingham, Y. Shao-Horn, Energy & Environmental Science 6 (2013) 750–768.
[9] J. Wang, Y. Li, X. Sun, Nano Energy 2 (2013) 443–467.
[10] C. Tran, X.-Q. Yang, D. Qu, Journal of Power Sources 195 (2010) 2057–2063.
[11] C. Tran, J. Kafle, X.-Q. Yang, D. Qu, Carbon 49 (2011) 1266–1271.
[12] Y. Li, X. Li, D. Geng, Y. Tang, R. Li, J.-P. Dodelet, M. Lefèvre, X. Sun, Carbon 64 (2013) 170–177.
[13] Y.C. Lu, H.A. Gasteiger, Y. Shao-Horn, J Am Chem Soc 133 (2011) 19048–19051.
[14] J. Yin, B. Fang, J. Luo, B. Wanjala, D. Mott, R. Loukrakpam, M.S. Ng, Z. Li, J. Hong, M.S. Whittingham, C.J. Zhong, Nanotechnology 23 (2012) 305404.
[15] T.T. Truong, Y. Liu, Y. Ren, L. Trahey, Y. Sun, Acs Nano 6 (2012) 8067–8077.
[16] J. Ming, Y. Wu, J.-B. Park, J.K. Lee, F. Zhao, Y.-K. Sun, Nanoscale 5 (2013) 10390–10396.
[17] M. Eswaran, N. Munichandraiah, L.G. Scanlon, Electrochemical and Solid-State Letters 13 (2010) A121.
[18] M. Yuasa, T. Matsuyoshi, T. Kida, K. Shimanoe, Journal of Power Sources 242 (2013) 216–221.
[19] Y. Zhao, L. Xu, L. Mai, C. Han, Q. An, X. Xu, X. Liu, Q. Zhang, Proceedings of the National Academy of Sciences 109 (2012) 19569–19574.
[20] E. Nasybulin, W. Xu, M.H. Engelhard, X.S. Li, M. Gu, D. Hu, J.-G. Zhang, Electrochemistry Communications 29 (2013) 63–66.
[21] H. Kitaura, H. Zhou, Advanced Energy Materials 2 (2012) 889–894.
[22] G.Q. Zhang, J.P. Zheng, R. Liang, C. Zhang, B. Wang, M. Hendrickson, E.J. Plichta, Journal of The Electrochemical Society 157 (2010) A953.
[23] J. Xiao, D. Mei, X. Li, W. Xu, D. Wang, G.L. Graff, W.D. Bennett, Z. Nie, L.V. Saraf, I.A. Aksay, Nano letters 11 (2011) 5071–5078.
[24] D. Higgins, Z. Chen, D.U. Lee, Z. Chen, Journal of Materials Chemistry A 1 (2013) 2639.
[25] D.S. Su, S. Perathoner, G. Centi, Chemical reviews 113 (2013) 5782–5816.
[26] J. Read, Journal of The Electrochemical Society 149 (2002) A1190–A1195.
[27] A. Débart, J. Bao, G. Armstrong, P.G. Bruce, Journal of Power Sources 174 (2007) 1177–1182.
[28] Y. Li, J. Wang, X. Li, D. Geng, M.N. Banis, R. Li, X. Sun, Electrochemistry Communications 18 (2012) 12–15.
[29] L. Qu, Y. Liu, J.-B. Baek, L. Dai, ACS nano 4 (2010) 1321–1326.
[30] D. Yu, Q. Zhang, L. Dai, Journal of the American Chemical Society 132 (2010) 15127–15129.
[31] Z. Yang, Z. Nie, X. a. Chen, X. Chen, S. Huang, Journal of Power Sources 236 (2013) 238–249.
[32] Z. Wu, W. Li, Y. Xia, P. Webley, D. Zhao, Journal of Materials Chemistry 22 (2012) 8835–8845.
[33] J. Li, N. Wang, Y. Zhao, Y. Ding, L. Guan, Electrochemistry Communications 13 (2011) 698–700.
[34] J. Yamashita, T. Hirano, M. Shioya, Carbon 40 (2002) 1541–1548.
[35] A.C. Lua, T. Yang, Journal of colloid and interface science 274 (2004) 594–601.
[36] H. Lv, N. Cheng, S. Mu, M. Pan, Electrochimica Acta 58 (2011) 736–742.
[37] S. Błażewicz, A. Świątkowski, B. Trznadel, Carbon 37 (1999) 693–700.
[38] Z.-M. Wang, H. Kanoh, K. Kaneko, G. Lu, D. Do, Carbon 40 (2002) 1231–1239.
[39] G. Wang, Z. Shao, Z. Yu, Nanotechnology 18 (2007) 205705.

[40] F. Huang, Q. Zhao, C. Luo, G. Wang, K. Yan, D. Luo, Chinese Science Bulletin 57 (2012) 4237–4243.

[41] H. Kang, G. Wang, H. Guo, M. Chen, C. Luo, K. Yan, Industrial & Engineering Chemistry Research 51 (2012) 7923–7931.

[42] W. Lu, A. Goering, L. Qu, L. Dai, Physical Chemistry Chemical Physics 14 (2012) 12099–12104.

[43] S.S. Zhang, X. Ren, J. Read, Electrochimica Acta 56 (2011) 4544–4548.

[44] J.S. Hummelshøj, J. Blomqvist, S. Datta, T. Vegge, J. Rossmeisl, K.S. Thygesen, A. Luntz, K.W. Jacobsen, J.K. Nørskov, The Journal of chemical physics 132 (2010) 071101.

[45] C.O. Laoire, S. Mukerjee, K. Abraham, E.J. Plichta, M.A. Hendrickson, The Journal of Physical Chemistry C 114 (2010) 9178–9186.

[46] M. Wang, L. Chen, L. Sun, Energy & Environmental Science 5 (2012) 6763.

[47] T. Maitra, S. Sharma, A. Srivastava, Y.-K. Cho, M. Madou, A. Sharma, Carbon 50 (2012) 1753–1761.

[48] X. Zheng, S. Zhang, J. Xu, K. Wei, Carbon 40 (2002) 2597–2603.

[49] M. Seredych, D. Hulicova-Jurcakova, G.Q. Lu, T.J. Bandosz, Carbon 46 (2008) 1475–1488.

[50] B. Vinayan, R. Nagar, V. Raman, N. Rajalakshmi, K. Dhathathreyan, S. Ramaprabhu, Journal of Materials Chemistry 22 (2012) 9949–9956.

[51] E.F. Vansant, P. Van Der Voort, K.C. Vrancken, Characterization and chemical modification of the silica surface, Elsevier, 1995.

[52] Z. Peng, S.A. Freunberger, L.J. Hardwick, Y. Chen, V. Giordani, F. Bardé, P. Novák, D. Graham, J.M. Tarascon, P.G. Bruce, Angewandte Chemie 123 (2011) 6475–6479.

[53] M. Hayashi, H. Minowa, M. Takahashi, T. Shodai, Electrochemistry 78 (2010) 325–328.

[54] M. Terrones, A.R. Botello-Méndez, J. Campos-Delgado, F. López-Urías, Y.I. Vega-Cantú, F.J. Rodríguez-Macías, A.L. Elías, E. Muñoz-Sandoval, A.G. Cano-Márquez, J.-C. Charlier, Nano Today 5 (2010) 351–372.

[55] J.-C. Charlier, Accounts of chemical research 35 (2002) 1063–1069.

[56] S.G. Louie, Electronic properties, junctions, and defects of carbon nanotubes, in: Carbon Nanotubes, Springer, 2001, pp. 113–145.